



# Selective conformer detection of short-lived base pair tautomers: A computational study of the unusual guanine-cytosine pairs using ultrafast resonance Raman spectroscopy

Baoling Tian<sup>a</sup>, Yizhou Fang<sup>a</sup>, Shulai Lei<sup>b,c,d,\*</sup>, Ke Xu<sup>b</sup>, Chaozheng He<sup>e,\*\*</sup>, Shujuan Li<sup>b,c</sup>, Hao Ren<sup>f,\*\*</sup>

<sup>a</sup> College of Chemistry and Pharmaceutical Sciences, Qingdao Agricultural University, Qingdao 266109, China

<sup>b</sup> Hubei Key Laboratory of Low Dimensional Optoelectronic Materials and Devices, Hubei University of Arts and Science, Xiangyang 441053, China

<sup>c</sup> Institute of Chemistry, Free University of Berlin, Arnimallee 22, Berlin D-14195, Germany

<sup>d</sup> Hubei Longzhong Laboratory, Xiangyang 441000, China

<sup>e</sup> Institute of Environment and Energy Catalysis, School of Materials Science and Chemical Engineering, Xi'an Technological University, Xi'an 710021, China

<sup>f</sup> School of Materials Science and Engineering, China University of Petroleum (East China), Qingdao 266580, China

## ARTICLE INFO

### Article history:

Received 22 November 2022

Revised 20 December 2022

Accepted 11 January 2023

Available online 13 January 2023

### Keywords:

Guanine-cytosine pair

Hydrogen bonding

Tautomer

Resonance Raman

Vibronic coupling

## ABSTRACT

Base pair mismatch has been regarded as the main source of DNA point mutations, where minor short-lived tautomers were usually involved. However, the detection and characterization of these unnatural species pose challenges to existing techniques. Here, by using systematic structural and ultrafast resonance Raman (RR) spectral analysis for the four possible conformers of guanine-cytosine base pairs, the prominent marker Raman bands were identified. We found that the hydrogen bonding vibrational region from 2300  $\text{cm}^{-1}$  to 3700  $\text{cm}^{-1}$  is ideal for the identification of these short live species. The marker bands provide direct evidence for the existence of the tautomer species, thus offering an effective strategy to detect the short-lived minor species. Ultrafast resonance Raman spectroscopy would be a powerful tool to provide direct evidence of critical dynamical details of complex systems involving protonation or tautomerization.

© 2023 Published by Elsevier B.V. on behalf of Chinese Chemical Society and Institute of Materia Medica, Chinese Academy of Medical Sciences.

Finding an effective strategy for conformer-selective detection of short-lived tautomer species is of pivotal importance to understand the biological processes of DNA in physiological environments. The maintenance of the genetic code relies on specific hydrogen bonding recognition between nucleic acid bases [1]. According to the Watson-Crick model, the guanine-cytosine base pairs (G:C) are stabilized by three hydrogen bonds as shown in Fig. 1a. This structural feature is important since it enables one to read the DNA sequence without unzipping the base pairs and is responsible for the recognition specificity and the binding patterns between other molecules and DNA strands [2,3]. The nucleic acid bases are well known to exhibit various tautomeric conformations in different environments, implying that DNA could

also accommodate a range of alternative pairing patterns that determines both the DNA double-helix structures and its biological function [4]. The “reverse Watson-Crick” minor tautomer ( $G^*:C^*$ ) shown in Fig. 1b is proposed according to the Löwdin hypothesis [5,6], which is believed to cause pairing mismatch and potentially is the main source of spontaneous point mutations. We adopt the initial structure of the  $G^*:C^*$  tautomer from the work by Fu *et al.* [7], which has been extensively examined as a source of mutagenic GC tautomers [8]. Other possible proton transferred tautomers were ruled out by structure optimizations and previous transition state calculations. While the noncanonical Hoogsteen guanine-cytosine base pairing ( $G:CH^+$ ) shown in Fig. 1d exists in the dynamic equilibrium with Watson-Crick conformation, which is sparsely populated ( $\sim 0.02\% - 0.4\%$ ) and short-lived (lifetimes  $\sim 0.2 - 2.5$  ms) [9]. The Hoogsteen  $G:CH^+$  can alter the base pair's electrostatics, constrict the DNA backbone, as well as play unique roles in DNA recognition [10]. The hydrogen bonding interaction in various transient guanine-cytosine base pairs produces the key aspects of both DNA structures and genetic-related features [11,12]. However, these transient isomers and the dynamic inter-

\* Corresponding author at: Hubei Key Laboratory of Low Dimensional Optoelectronic Materials and Devices, Hubei University of Arts and Science, Xiangyang 441053, China.

\*\* Corresponding authors.

E-mail addresses: [slei@hbuas.edu.cn](mailto:slei@hbuas.edu.cn) (S. Lei), [hecz2019@xatu.edu.cn](mailto:hecz2019@xatu.edu.cn) (C. He), [renh@upc.edu.cn](mailto:renh@upc.edu.cn) (H. Ren).

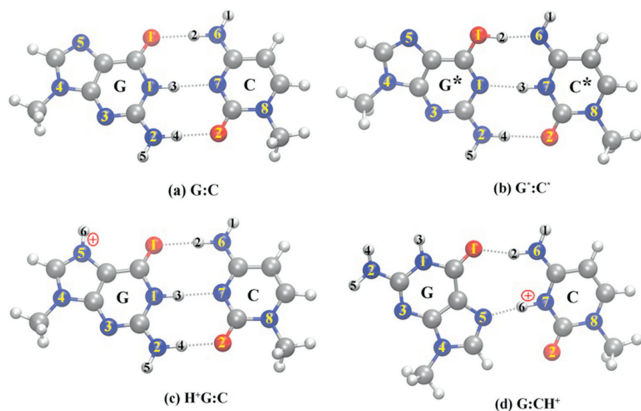


**Fig. 1.** Optimized geometries of the guanine–cytosine (with assigned labels) considered in this work: (a) Canonical Watson–Crick G:C, (b) the rare Watson–Crick tautomer G\*:C\*, (c) the protonated Watson–Crick H<sup>+</sup>G:C, and (d) the noncanonical Hoogsteen G:CH<sup>+</sup>. Silver, blue, red and white balls denote carbon, nitrogen, oxygen and hydrogen atoms, respectively.

conversions between them are difficult to detect due to the intrinsic complexities of the complexity and the fast kinetics in biological systems. Conventional crystalline characterizations are usually affected by crystallographic environments. Several crystalline experiments showed evidences of the existence of Hoogsteen G:CH<sup>+</sup>, however, solution nuclear magnetic resonance (NMR) characterizations suggest the same systems are Watson–Crick G:C conformation, implying that crystalline structures deviate from those *in vivo* [13]. In addition, the dynamic nature poses extra challenges for the detection and characterization of these short-lived conformers.

Some insights into these rare species are conventionally obtained by using X-ray crystal diffraction (XRD), infrared (IR) and/or Raman spectroscopy and mass spectrometry [14–16]. However, these detections are usually not performed *in vitro*, leading to ambiguities related to physiological functions. In addition, these techniques usually have temporal resolutions much lower than the fast binding kinetics. For instance, NMR relaxation dispersion experiments have successfully detected Hoogsteen G:CH<sup>+</sup> in small, naked DNA duplexes [17], but it is difficult to characterize large DNA/protein complexes, due to severe spectral overlaps and unfavorable relaxations. There are a number of successful characterizations of the short-lived or sparsely populated guanine–cytosine tautomers [18], but they are incapable of capturing the atomic resolution structures, and the tautomerization dynamics are not clear.

An effective tool to selectively detect G:C in a mixture with its transient tautomers would greatly facilitate the understanding of the microscopic mechanism and related biological functions. Spontaneous resonance Raman (spRR) spectroscopy detects the vibronic coupling between molecular vibrations and electronic transitions, and is a powerful technique to provide molecular fingerprint information [19–22]. Molecular vibrations are sensitive to local chemical environments and their resonance with electronic transitions provides a high signal-to-noise ratio [23–26]. By tuning the excitation wavelengths, spRR is capable of probing specific basepairs during complex biological processes. Combined with ultrafast pulses, spRR has been extended to the time domain, i.e., stimulated resonance Raman (stRR), which can give kinetic information of fast biological processes [27,28]. With these advantages, spRR and stRR are powerful tools for identifying base-pair species probably with short lifetimes or only exist transiently.

In this work, we carried out systematic *ab initio* simulations to study the spRR and ultrafast stRR spectra of the four biologically important guanine–cytosine conformers, i.e., G:C, G:CH<sup>+</sup>, G\*:C\* and H<sup>+</sup>G:C. G:C is the most populated Watson–Crick conformation,

while the Hoogsteen G:CH<sup>+</sup> exists in dynamic equilibrium with canonical G:C. The rare tautomers G\*:C\* and H<sup>+</sup>G:C, which might participate in DNA mutation, were also considered here. The characteristic RR spectral patterns, as well as the appropriate excitation wavelengths for resonance enhancement, were predicted and would serve as references for future experiments. The spRR signals were evaluated by calculating the differential Raman scattering cross section [29]:

$$S^{sp}(\omega_{in}, \omega_{sig}) = \frac{d\sigma}{d\Omega} \propto \sum_{c,a} P(a) |\alpha_{ca}(\omega_{in})|^2 \delta(\omega_{in} - \omega_{sig} - \omega_{ca}) \quad (1)$$

where  $\omega_{in}$  is the incident frequencies, while  $\omega_{sig}$  is the Raman signal frequencies.  $P(a)$  denotes the population of the state  $|a\rangle$ .  $\alpha_{ca}(\omega_{in})$  is the polarizability between state  $|a\rangle$  and  $|c\rangle$ , which explicitly depends on the incident frequency  $\omega_{in}$ . In the practical calculations, the delta function  $\delta(\omega_{in} - \omega_{sig} - \omega_{ca})$  is replaced by a Gaussian function, which can ensure energy conservation during the scattering process. The pump-probe stRR signals can be obtained by:

$$S^{st}(\Omega_1) = \sum_{ac} P(a) \frac{i\alpha_{ac}^{(1)} \left[ \alpha_{ac}^{(2)} - (\alpha_{ac}^{(2)})^* \right]}{\Omega_1 - \omega_{ca} + i\Gamma} \quad (2)$$

Here  $\alpha_{ac}^{(1)}$  is the effective transition polarizability between the state  $|a\rangle$  and  $|c\rangle$ , which is given by

$$\alpha_{ac}^{(i)} = \frac{1}{\pi} \sum_b \langle a|b\rangle \langle b|c\rangle |\mu_{eg}|^2 \int_{-\infty}^{+\infty} d\omega \frac{E_i^*(\omega) E_i(\omega + \omega_{ac})}{\omega - \omega_i - \omega_{bc} + i\Gamma_b} \quad (3)$$

Here  $\omega_i$  and  $E_i(\omega)$  denote the center frequency and envelope of the  $i$ th pulse, respectively. Detailed derivations of spRR and stRR can be found in Ref. [29]. Considering the electronic dynamics is much faster than the nuclear relaxation, we use the linewidth parameters of 10 cm<sup>-1</sup> and 100 cm<sup>-1</sup> for the vibrational and electronic spectra to capture the broadening effects originating from intermediate state lifetimes. These values have been widely used in previous theoretical calculations [30–33]. The calculated vibrational frequencies were scaled by 0.97 to correct the systematic errors [34]. All the calculations, including structure optimization, vibrational analysis and electronic transitions were carried out by using the Gaussian 16 package at the (time-dependent) B3LYP/cc-pVTZ level of theory [35]. This computational scheme has been proven successful to describe the electronic structures of nucleobases [36]. To understand the strong peaks in the UV absorption spectra, we performed natural transition orbital (NTO) analysis for the corresponding electronic transitions [37]. The first order Franck-Condon contribution to the vibronic coupling was considered, while the higher order Herzberg-Teller terms were neglected since only strongly allowed electronic transitions were involved [38,39]. The solvation effect was implicitly accounted by the polarizable continuum model with conductor-like solvations (CPCM) method [40].

Fig. 1 shows the fully optimized structure of the guanine–cytosine base pairs. The Watson–Crick pairing pattern has three hydrogen bonds, while the Hoogsteen structure has only two. Three kinds of hydrogen bonds in G:C are shown in Fig. 1a, one proton is covalently bonded to N1 of guanine and hydrogen bonded to N7 of cytosine, the second hydrogen bond occurs between the amino group of cytosine and the O1 of guanine, and the third hydrogen bond occurs between the amino group of guanine and the O2 of cytosine. The Hoogsteen G:CH<sup>+</sup> pairing pattern is stabilized by two hydrogen bonds resulting from a 180° rotation of the purine base in Watson–Crick. As shown in Fig. 1d, one proton is bonded to N7 of cytosine and N5 of guanine, and the second hydrogen bond occurs between the amino group of cytosine and the O1 of guanine. The formation of two hydrogen bonds shortens the C–C distance between guanine and cytosine, which

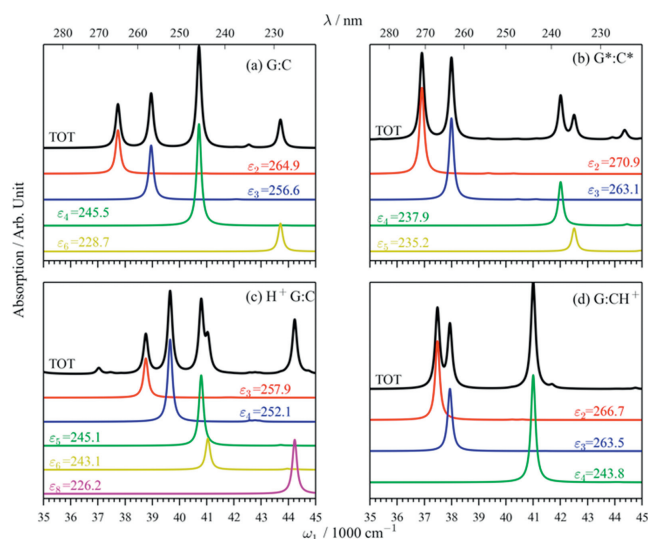


**Fig. 2.** Vibration resolved UV-vis absorption spectra for four guanine-cytosine conformers.

can lead to the kinks of the DNA double helix. Herein, except for the biologically important Watson-Crick G:C and Hoogsteen G:CH<sup>+</sup> conformation, we extend the selected analogs including the “reverse Watson-Crick” minor tautomer G\*:C\* and the isolated protonated Watson-Crick H<sup>+</sup>G:C. The G\*:C\* species is a double proton transfer state of G:C. As shown in Fig. 1b, the guanine exists in its enol form (G\*), and the cytosine exists in the form of iminocytosine (C\*). The hydrogen bonds of G\*:C\* are covalently bound to O1 of guanine and the N7 of cytosine, respectively. This short-lived G\*:C\* tautomer is considered to be the main potential source of spontaneous point mutations. But there is no direct experimental evidence to probe this isomer so far. Accessing its spectroscopic signatures would facilitate the investigation of the proton transfer mechanism on DAN mutation. The protonated H<sup>+</sup>G:C as shown in Fig. 1c, mainly existing in solution at pH 5.8 [41,42], is one base pairing conformer of the protonated DNA, which is very important for a better understanding of DNA biological chemistry. Here, both the canonical G:C and the double proton transfer conformer G\*:C\* are neutral structures, while the protonated H<sup>+</sup>G:C and the proton-bound non-covalent G:CH<sup>+</sup> are with net charges +1, respectively. To reduce the computational cost of the simulations without affecting the spectroscopic properties, the methyl groups were used to instead the binding sites at N8 of cytosine and N4 of guanine in guanine-cytosine isomers, which is bound to ribose or deoxyribose in nucleic acids.

Appropriate excitation wavelengths are required to match the UV absorption of the target species for UVRD detection. It can be obtained by examining the vibrational resolved UV absorption spectroscopy of guanine-cytosine. As shown in Fig. 2, the total absorption and the dominant contributions of the main peaks of each conformer were depicted in 222–286 nm (35,000–45,000 cm<sup>-1</sup>) region, which match well with the experimental UV-vis absorption spectra of nucleotides [43]. Herein, we also assessed the spatial distribution of the strongly allowed electronic excitations by performing NTO analysis. The NTO plots of the interesting electronic transitions of the four conformers are presented in Figs. S1–S4 (Supporting information). For clarity, we denote the *i*th electronic transition of isomers S as  $\epsilon^S_i$ . The total absorption spectra are plotted in black.

As shown in Fig. 2a, four electronic transitions have been identified as contributing significantly to the total UV-vis spectrum of the canonical G:C. The maximum peak lies near 40,726 cm<sup>-1</sup>

(245.5 nm), which is mainly attributed to the electron rearrangement transition of  $\epsilon^I_4$  from guanine to cytosine. It contains considerable hydrogen bond distribution changes around the N6H2, N1H3, and N2H4 regions along with the NTO analysis in Fig. S1. Two weak absorption bands at 37,747 cm<sup>-1</sup> (264.9 nm) and 38,968 cm<sup>-1</sup> (256.6 nm) are comparable in intensity. One is contributed from the  $\epsilon^I_2$  excitation at 37,747 cm<sup>-1</sup>, which is ascribed to the electron rearrangement inside the guanine base, while the second band at 38,968 cm<sup>-1</sup> comes from a typical electron rearrangement transition of  $\epsilon^I_3$  inside the cytosine base. The spatial distributions of the NTOs for these transitions are depicted in Fig. S1. The fourth transition  $\epsilon^I_6$  is located in the 228.7 nm region, which is a weak transition.

G\*:C\* is the double proton transfer state from G:C. Two main peaks appear at 36,921 cm<sup>-1</sup> (270.9 nm) and 38,007 cm<sup>-1</sup> (263.1 nm), respectively. One comes from the  $\pi \rightarrow \pi^*$  transition of  $\epsilon^{II}_2$  excitation at 270.9 nm and another peak arises from the  $\epsilon^{II}_3$  excitation at 263.1 nm. Herein,  $\epsilon^{II}_2$  is a typical electron rearrangement inside guanine, and  $\epsilon^{II}_3$  is the typical electron rearrangement inside cytosine as shown in Fig. S2. Compared to G:C, there are no obvious peaks in the 240–260 nm region. Two relatively weaker shoulder bands are observed at 237.9 nm and 235.2 nm, which are corresponding to the excitation of  $\epsilon^{II}_4$  at 42,020 cm<sup>-1</sup> (237.9 nm) and  $\epsilon^{II}_5$  at 42,463 cm<sup>-1</sup> (235.2 nm). These two excitations arise from the electron rearrangement from guanine to cytosine as shown in Fig. S2. It is worth noticing that the electron rearrangement excitations from guanine to cytosine in G\*:C\* exhibit some blueshift compared to that of G:C, while the electron rearrangement excitations inside guanine ( $\epsilon^{II}_2$ ) and cytosine ( $\epsilon^{II}_3$ ) exhibit some redshift, which are in agreement with the proposing hyperchromic effect or subtractive effect.

For the H<sup>+</sup>G:C conformer, the protonation has a significant effect on its absorption spectrum. As shown in Fig. 2c, there are no obvious bands in the region above 260 nm. Comparatively, the peaks are more dense and concentrated in the region 240–260 nm, which are respectively centered at 38,772 cm<sup>-1</sup>, 39,664 cm<sup>-1</sup> and 40,808 cm<sup>-1</sup>. According to the corresponding NTO analysis (Fig. S3), these peaks at 38,772 cm<sup>-1</sup> and 39,664 cm<sup>-1</sup> are assigned from the contributions of  $\epsilon^{IV}_3$  at 257.9 nm and  $\epsilon^{IV}_4$  at 252.1 nm, which are related to the electron rearrangement from guanine to cytosine. While the other two peaks at 40,808 cm<sup>-1</sup> and 41,054 cm<sup>-1</sup> are assigned to the contributions of  $\epsilon^{IV}_5$  at 245.1 nm and  $\epsilon^{IV}_6$  at 243.6 nm, which are typically considered the electron rearrangement from cytosine to guanine. In addition, there is a strong peak in the deep UV region at 40,808 cm<sup>-1</sup>, which is assigned to the electron rearrangement inside the cytosine base by  $\epsilon^{IV}_8$  excitation at 226.2 nm. These characteristic features suggest that the protonated H<sup>+</sup>G:C represents important uniqueness, which may contribute to the detection of H<sup>+</sup>G:C.

As the purine of G:C is rotated 180°, one proton of guanine is covalently bound to the N7 of the cytosine to form G:CH<sup>+</sup>. As shown in Fig. 2d, the Hoogsteen G:CH<sup>+</sup> spectra feature also has three typical absorption peaks, which are generally similar to the Watson-Crick G:C. The strongest band appears is corresponding to the contributions of  $\epsilon^{III}_4$  at 41,017 cm<sup>-1</sup> (243.8 nm), while two weaker transitions appear above 260 nm. The strongest peak of G:CH<sup>+</sup> at 243.8 nm displays some blue-shift compared to that of G:C at 245.5 nm, while other two weak peaks of G:CH<sup>+</sup> above 260 nm show some red-shifts. In addition, two weak peaks are also dramatically reweighted in the relative intensities in G:CH<sup>+</sup>. One peak located at 37,495 cm<sup>-1</sup> (266.7 nm) is stronger than that at 37,951 cm<sup>-1</sup> (263.5 nm). The former peak assigned to  $\epsilon^{III}_2$  mainly comes from the contribution of N7-H6 stretching, while the weaker  $\epsilon^{III}_3$  peak is mainly assigned to the N1-H3 stretching, which is in agreement with the NTOs analysis of these electronic excitations depicted in Fig. S4. Spectroscopically, we cannot directly

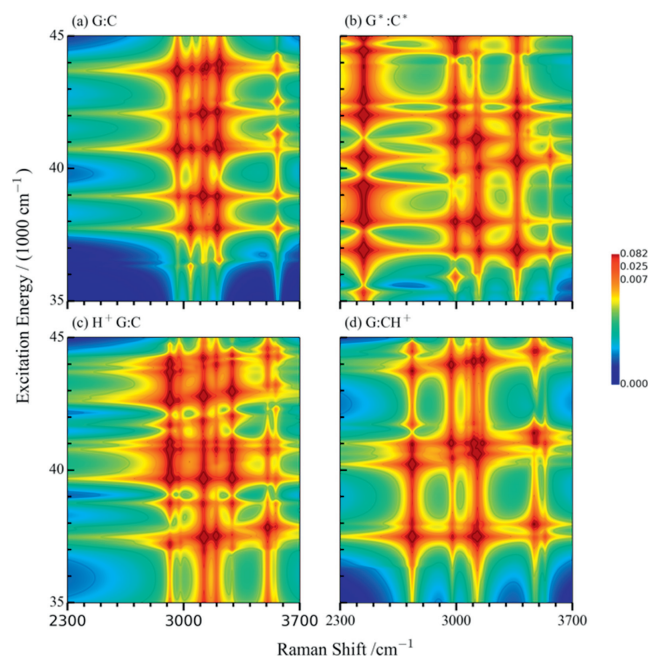


**Fig. 3.** Two-dimensional spontaneous Raman spectra of (a-d) four guanine-cytosine conformers with excitation energy scanned from 35,000  $\text{cm}^{-1}$  to 45,000  $\text{cm}^{-1}$ . The horizontal and vertical axes represent the Raman shift and excitation energy, respectively.

distinguish four conformers alone due to the congestion of their UV-vis spectrum, but these spectral data provide the basis necessary for further exploitation of UVR spectroscopy.

To illustrate the capability of RR to characterize the pairing patterns of guanine-cytosine conformers, the correlation between the structural components and their RR spectroscopic signatures is established. According to the structural analysis, the hydrogen-bonding interaction modes, especially the CH/NH/OH modes in the hydrogen-bonding interactions region from 2300  $\text{cm}^{-1}$  to 3700  $\text{cm}^{-1}$ , are the key RR active modes. They are far away from the normal vibrational frequencies of the guanine or cytosine monomer, and can be effectively filtered out from the vibrational modes of  $\text{H}_2\text{O}$  or peptides by tuning the incoming excitation wavenumber. These properties make these hydrogen-bond related vibrational modes have unexpected marking effects in structural diagnosis, which can benefit experimental applications in spectroscopy detection. These well-defined RR marker bands under the UV resonance excitation have been assessed as shown in Fig. 3. Tables 1–4 present the Raman active vibrational modes with relatively obvious intensity in the range 2300–3700  $\text{cm}^{-1}$  under the excitation from 35,000–45,000  $\text{cm}^{-1}$ . There are also other vibra-

**Table 1**

Raman active modes and assignments of G:C. All frequencies are wavenumbers.

Frequency ( $\text{cm}^{-1}$ )	Assignment
2960	G: C-H stretching inside $\text{CH}_3$
2968	C: C-H stretching in $\text{CH}_3$
3041	G: N1-H3 stretching
3114 (3132)	C: C-H stretching
3139	G: C-H stretching
3202	G:N2-H4 stretching (mainly) coupled with C:N6-H2 stretching
3215	C:N6-H2 stretching (mainly) coupled with G:N2-H4 stretching
3562	C:N6-H1 stretching
3566	G:N2-H5 stretching

**Table 2**

Raman active modes assignments for  $\text{G}^*:\text{C}^*$ . All frequencies are wavenumbers.

Frequency ( $\text{cm}^{-1}$ )	Assignment
2440	G: O1-H2 stretching
2959	G: C-H stretching in $\text{CH}_3$
2969	C: C-H stretching in $\text{CH}_3$
2993	C: N7-H3 stretching
3117	C: C-H stretching
3366	G:N2-H4 symmetric stretching
3431	C:N6-H1 stretching
3565	G:N2-H5 stretching

**Table 3**

Raman active modes and assignments for  $\text{H}^+\text{G}:\text{C}$ . All frequencies are wavenumbers.

Frequency ( $\text{cm}^{-1}$ )	Assignment
2917	G: N1-H3 stretching
3116 (3135)	C: C-H stretching
3122	G: N2-H4 stretching
3196	G: C-H stretching
3292	C: N6-H2 stretching
3506	G: N5-H6 stretching
3555	G: N2-H5 free stretching

tion modes, which did not include in these Table lists, but they are all RR-silent or with weaker intensity in this excitation region.

Using the marker bands of G:C as a benchmark, prominent UVR bands of its short-live tautomers are evaluated at each excitation wavelength. As shown in Fig. 3a, five well-separated vibrational modes are observed under the resonant excitation from 35,000  $\text{cm}^{-1}$  to 45,000  $\text{cm}^{-1}$ , which can be conveniently classified into two categories. One is originated from the C-H stretching, such as the C-H stretching of  $\text{CH}_3$  inside guanine at 2960  $\text{cm}^{-1}$ , and the C-H stretching of guanine or cytosine at 3139 or 3115  $\text{cm}^{-1}$ . Another special signal band comes from the N-H stretching, including the N-H stretching inside the hydrogen bonds and the free N-H stretching. Such as both the G:N1-H3 stretching at 3041  $\text{cm}^{-1}$ , the G:N2-H4 stretching at 3203  $\text{cm}^{-1}$ , and the C:N6-H2 stretching at 3215  $\text{cm}^{-1}$  are all the N-H stretching involved to the hydrogen bonds, while both the G:N2-H5 stretching at 3567  $\text{cm}^{-1}$  and the C:N6-H1 stretching at 3563  $\text{cm}^{-1}$  are free N-H stretching. Compared to free N-H stretching around 3500  $\text{cm}^{-1}$ , all the hydrogen bonds related N-H stretching centered from 3000  $\text{cm}^{-1}$  to 3200  $\text{cm}^{-1}$  are blue-shifted, which can be selectively identified by the  $\epsilon^1_2$  resonant excitation at 264.9 nm (37,750  $\text{cm}^{-1}$ ). It can also be confirmed by the NTO analysis of G:C (Fig. S1). As the most population conformation, the Watson-Crick G:C will be considered as the reference standard in the following RR spectral discussion.

To confirm its tautomeric conformer, we further investigate the spRR spectra of  $\text{G}^*:\text{C}^*$ . As shown in Fig. 3b, one strong signal at 2440  $\text{cm}^{-1}$  exhibits strong Raman intensity, while bands of medium intensity are observed at 2993, 3117(3136), 3366 and

**Table 4**

Raman active modes and assignments for  $\text{G}:\text{CH}^+$ . All frequencies are wavenumbers.

Frequency ( $\text{cm}^{-1}$ )	Assignment
2733	C: N7-H6 stretching
2969	G: C-H stretching in $\text{CH}_3$
2976	C: C-H stretching in $\text{CH}_3$
3105	C: N6-H2 stretching
3152(3127)	C: C-H stretching
3157	C: C-H stretching
3468	G: N1-H3 stretching
3484	G: H4-N2-H5 symmetric stretching
3534	C: N6-H1 stretching
3595	G: H4-N2-H5 asymmetric stretching

3565(3431)  $\text{cm}^{-1}$ . This is different from that of canonical G:C, especially the G:O1-H2 stretching at 2440  $\text{cm}^{-1}$ , which is formed by the hydrogen bonded to N6 of cytosine, and belongs to the marker RR band of G\*:C\*. This peak is the strongest signal for G\*:C\* under the selected excitation range, which is the direct evidence for the formation of transient G\*:C\*. Meanwhile, as the atom H3 inside guanine undergoes proton transfer, a new N7-H3 bond is formed inside G\*:C\*, and its characteristic Raman signal N7-H3 stretching appears at 2993  $\text{cm}^{-1}$ , which exhibits a redshifted compared with the G:N1-H3 stretching at 3041  $\text{cm}^{-1}$  inside G:C. It is also a characteristic RR peak for G\*:C\*. That means if the G\*:C\* is present at physiological conditions, both a strong RR signal band around 2440  $\text{cm}^{-1}$  and a weaker peak around 2993  $\text{cm}^{-1}$  would be observed under specific electronic excitation. The full assignment of the other three assigned RR bands, such as the C:C-H stretching at 3117  $\text{cm}^{-1}$ , the G:N2-H4 symmetric stretch at 3366  $\text{cm}^{-1}$ , and the free N-H stretching at 3431  $\text{cm}^{-1}$  (C:N6-H1 stretching) or 3566  $\text{cm}^{-1}$  (G:N2-H5 stretching) are listed in Table 3, which are also valuable for the detection of G\*:C\*. For example, the G:N2-H4 stretching at 3366  $\text{cm}^{-1}$  in G\*:C\* has some blue-shift compared to that of G:C at 3202  $\text{cm}^{-1}$ . Based on the analysis of the vertical excitation energy, both  $\varepsilon^{\text{IV}}_2$  at 270.9 nm (36,921  $\text{cm}^{-1}$ ) and  $\varepsilon^{\text{IV}}_4$  at 238.0 nm (42,020  $\text{cm}^{-1}$ ) can be selected as the preferred excitation wavelengths to identify G\*:C\*. Under this excitation, the specific RR peaks at 2240  $\text{cm}^{-1}$  and 3366  $\text{cm}^{-1}$  can be well identified, which are much stronger than the C-H stretching signals. This is consistent with the NTOs analyses of  $\varepsilon^{\text{IV}}_2$  and  $\varepsilon^{\text{IV}}_4$  for G\*:C\* shown in Fig. S2.

H<sup>+</sup>G:C is the protonated conformer of G:C under a low pH environment, in which one proton is bound to the N5 of guanine. Different from G\*:C\*, there are no obvious Raman bands in the low-frequency region below 28,000  $\text{cm}^{-1}$ . In the high-frequency region above 3400  $\text{cm}^{-1}$ , H<sup>+</sup>G:C shows another intense Raman band at 3506  $\text{cm}^{-1}$  in addition to the free G:N2-H5 stretching at 3555  $\text{cm}^{-1}$ , which is assigned to the G:N5-H6<sup>+</sup> stretching. It is a characteristic marker RR band of H<sup>+</sup>G:C. In the medium region from 2900 to 3300  $\text{cm}^{-1}$ , the spRR spectrum shows several identical vibrational modes attributable to hydrogen bond interaction, such as the G:N1-H3 stretching at 2917  $\text{cm}^{-1}$ , G:N2-H4 stretching at 3122  $\text{cm}^{-1}$ , and C:N6-H2 stretching at 3292  $\text{cm}^{-1}$ . Due to the strong ion-induced dipole interaction, three typical hydrogen-bond related modes exhibit obvious red or blue shift, such as that the G:N1-H3 stretching is red-shifted from 3042 to 2917  $\text{cm}^{-1}$ , the G:N2-H4 stretching is red shifted from 3202 to 3122  $\text{cm}^{-1}$ , and the C:N6-H2 stretching is blue-shifted from 3216 to 3292  $\text{cm}^{-1}$ . Moreover, the spRR signal bands of H<sup>+</sup>G:C is more separated compared to that of G:C.

G:CH<sup>+</sup> is stabilized by two hydrogen bonds, with the bond donors being the N6 and N7 of cytosine and acceptors being the O1 and N5 of guanine, respectively. As a result, both the C:N7-H6 stretching at 2733  $\text{cm}^{-1}$  and the C:N6-H2 stretching at 3105  $\text{cm}^{-1}$  are the typical marker bands to characterize G:CH<sup>+</sup>. Meanwhile, as the broken of three hydrogen bonds in G:C, one free N1-H3 bond is released. As shown in Fig. 3d, three N-H stretching modes, such as the free G:N1-H3 stretching at 3468  $\text{cm}^{-1}$ , the G:H4-N2-H5 symmetric stretching at 3484  $\text{cm}^{-1}$  and the G:H4-N2-H5 asymmetric stretching at 3495  $\text{cm}^{-1}$  are also observed. All these characteristic RR bands can be well identified under the special electronic excitation. For example, both the C:N7-H6 stretching at 2733  $\text{cm}^{-1}$  and C:N6-H2 stretching at 3105  $\text{cm}^{-1}$  can be well identified under the  $\varepsilon^{\text{IV}}_2$  excitation at 266.7 nm (37,495  $\text{cm}^{-1}$ ), the G:N1-H3 stretching at 3468  $\text{cm}^{-1}$  is a RR active mode under the  $\varepsilon^{\text{IV}}_3$  excitation at 263.5 nm (37,951  $\text{cm}^{-1}$ ). Compared to that of G\*:C\*, even a similar N7-H6 bond is also appeared in G:CH<sup>+</sup>, but the corresponding G:N7-H6 stretching signals are red shifted from 2993 to 2733  $\text{cm}^{-1}$ , which is far away from the noise C-H stretching and

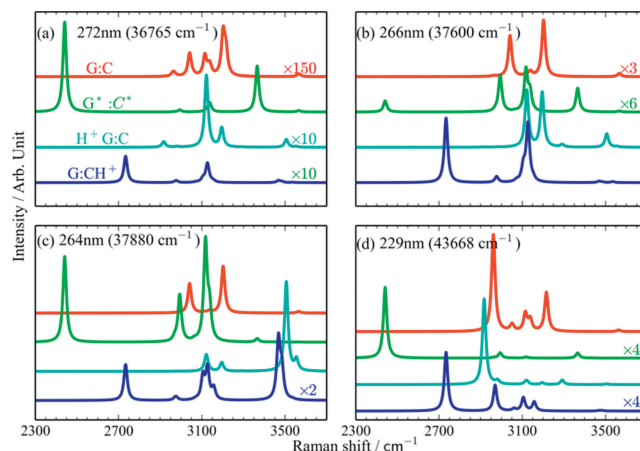


**Fig. 4.** One-dimensional spontaneous Raman spectra of G:C (red), G\*:C\* (green), H<sup>+</sup>G:C (cyan) and G:CH<sup>+</sup> (blue) species. The excitation energies are selected at (a) 272, (b) 266, (c) 264 and (d) 229 nm.

makes the identification of G:CH<sup>+</sup> conformer much easily. The spatial distribution of the NTOs for  $\varepsilon^{\text{IV}}_2$ ,  $\varepsilon^{\text{IV}}_3$  and  $\varepsilon^{\text{IV}}_4$  are depicted in Fig. S4. Herein, the electronic transition  $\varepsilon^{\text{IV}}_2$  is related to the N7-H6 bond with an O2 to N7 transition, the electronic transition  $\varepsilon^{\text{IV}}_3$  is mainly related to the electronic transition localized around N1-H3 bond, and the electronic transition  $\varepsilon^{\text{IV}}_4$  is mainly related to the electronic transition localized around N6-H2 bond, which are all in better agreement with the typical spRR signals.

The UVRR spectra of H<sub>2</sub>O and D<sub>2</sub>O solutions of nucleosides (dA, dG, dC, dT) have been extensively studied under the laser excitation wavelengths in the deep UV region from 193 nm to 280 nm [44–46]. The results show that the RR spectral signal are strongly dependent on excitation wavelength and constitute sensitive and selective probe for nucleosides. To characterize the prominent Raman bands that could potentially be used to identify different short-lived tautomer species, we studied the spRR spectra of four conformers excited at selected excitation wavelengths of 272, 266, 264 and 229 nm.

Fig. 4a compares UVRR spectra of G:C, G\*:C\*, H<sup>+</sup>G:C, and G:CH<sup>+</sup> excited at 272 nm. The dominant bands at 2440  $\text{cm}^{-1}$  exhibits the outstanding Raman intensity in G\*:C\*, which is well isolated from other UVRR markers under this excitation. This band is assigned to the mode involving of G:O1-H2 stretching in G\*:C\*. Another typical band of G\*:C\* occurs at 3366  $\text{cm}^{-1}$ . It's assigned to a G:N2-H4 stretching, which exhibits a moderately Raman intensity. These are useful marker Raman bands of G\*:C\*, which provide a unique advantage in discriminating the G\*:C\*. In contrast, G:C excited at 272 nm exhibits the weakest signal intensities, roughly lower than 150 orders of magnitude of G\*:C\*, while both the H<sup>+</sup>G:C and G:CH<sup>+</sup> exhibit relatively weak Raman signals.

Fig. 4b shows the UVRR spectra excited at 266 nm. G:CH<sup>+</sup> gives a well-resolved band at 2733  $\text{cm}^{-1}$  assigned to the C:N7-H6 stretching. It's well isolated from markers of other species. Another typical band of G:CH<sup>+</sup> occurs at 3105  $\text{cm}^{-1}$  due to C:N6-H2 stretching. These markers are well resolved, which are useful marker bands for diagnosing G:CH<sup>+</sup>. It is worth noting that a weak band at 3506  $\text{cm}^{-1}$  of H<sup>+</sup>G:C under 266 nm excitation exhibits a strong signal under excitation at 264 nm (Fig. 4c). It corresponds to the G:N5-H6<sup>+</sup> stretching of H<sup>+</sup>G:C, which provides a potentially valuable indicator of H<sup>+</sup>G:C. The results show that UVRR signals of the G:C and its short-lived tautomer species are strongly dependent on excitation wavelength and constitute a sensitive and selective detection of the labeled bands. We also investigated the spectral signal under excitation at 229 nm, a common excitation wavelength in experiments. As shown in Fig. 4d, both G:C and

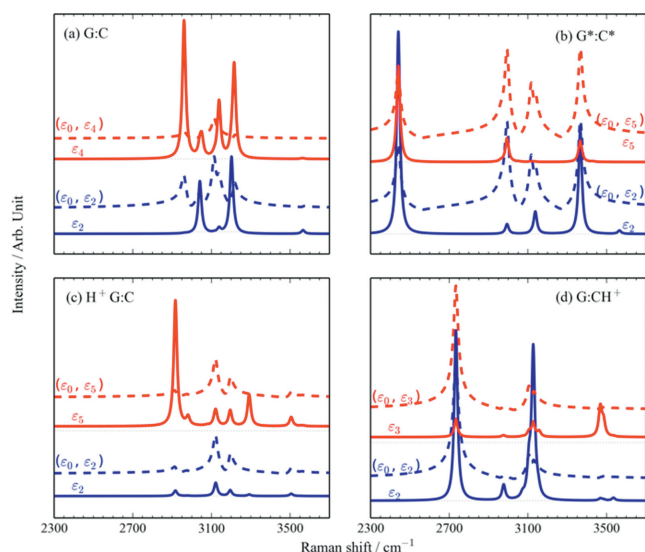


**Fig. 5.** Comparison between stRR (dashed) and spRR (solid) spectra for (a) G:C, (b) G\*:C\*, (c) H<sup>+</sup>G:C and (d) G:CH<sup>+</sup> BPs. The center frequencies of the pump and probe pulse used in the stRR simulation are denoted as ( $\varepsilon_0$ ,  $\varepsilon_i$ ), with the pump chosen to be pre-resonant at  $\varepsilon_0 = 25,000 \text{ cm}^{-1}$ .

H<sup>+</sup>G:C species exhibited stronger UVRR signals compared to the other two species. A typical marker band for both G:C and H<sup>+</sup>G:C is the G:N1-H3 stretching, which appears at  $2960 \text{ cm}^{-1}$  in G:C, but shifts to  $2916 \text{ cm}^{-1}$  in H<sup>+</sup>G:C. Both G\*:C\* and G:CH<sup>+</sup> exhibited weaker UVRR signals, but also provided well-resolved marker bands at  $2440 \text{ cm}^{-1}$  and  $2733 \text{ cm}^{-1}$ , respectively.

As mentioned above, the protonated H<sup>+</sup>G:C and G:CH<sup>+</sup> can be effectively identified under excitation at 266 and 264 nm, while the excitation wavelength of 272 nm is a suitable excitation energy to enhance the G\*:C\* signals. These results provide a library of UVRR labeled bands for structural analysis of guanine–cytosine undergoing protonation or tautomerization events.

Different from spRR, time-resolved stimulated resonance Raman (stRR) is a nonlinear technique using a pump-probe pulse configuration that drives the system to evolve in its vibrationally excited states, which can directly probe the structural dynamics along their vibrational modes and has a sufficiently high temporal resolution to capture spectroscopic snapshots for short-lived tautomer species. The pump pulse prepares a vibrationally excited state wave packet in the ground electronic state via a pre-resonance Raman process, and the probe pulse arrives the sample after a time delay to probe the dynamics of this wave packet with a resonance Raman process. This pulse configuration preserves the selectivity and resonant enhancement of spRR, in the meantime, avoiding the excited state population probably caused by the pump. A strong signal in the stRR spectra implies that the corresponding vibrational excitation survives the time delay between the pump and probe pulses and hence produces a strong correlation. Fig. 5 presents the one-dimensional (1D) stRR results simulated to illustrate the applicability of this technique in conformer-selective detection. The pump was chosen to be centered at  $\varepsilon_0 = 25,000 \text{ cm}^{-1}$ , which is off-resonant with any excited states of four GC conformers. The probe is chosen to be resonant with the selected electronic excitation for each system denoted as  $i$ . The center frequencies of the pump and probe pulse used in the stRR simulation are denoted as ( $\varepsilon_0$ ,  $\varepsilon_i$ ).

The 1D stRR spectra (dashed line) accompanied with the frequency-domain spontaneous version (solid lines) are shown in Fig. 5. Similar to the spRR signals, the stRR can capture the distinctive features of four species, ensuring their capability for struc-

ture characterization, such as that both the G:O1-H2 stretching of G\*:C\* at  $2440 \text{ cm}^{-1}$  and the marker C: N7-H6<sup>+</sup> stretching of G:CH<sup>+</sup> at  $2733 \text{ cm}^{-1}$  are all identified under the special stRR simulation. However, the relative intensities of the marker peaks change obviously. As shown in Fig. 5a, the prominent spectral indicative of stRR for G:C is an intense Raman band at  $3114 \text{ cm}^{-1}$ , which involves C–H stretching of cytosine under the excitation  $\varepsilon^I_2$ , while the maximum intensity bands turn to the G:N2-H4 stretching at  $3202 \text{ cm}^{-1}$  in the spRR detection. For G\*:C\* as shown in Fig. 5b, in addition to the marker band at  $2440 \text{ cm}^{-1}$ , both the C:N7-H3 stretching at  $2993 \text{ cm}^{-1}$  and C:C–H stretching at  $3117 \text{ cm}^{-1}$  exhibit relatively more intensities in the stRR detection compared to that of spRR. Similarly, H<sup>+</sup>G:C presents an intense band around  $2916 \text{ cm}^{-1}$  under the  $\varepsilon^{\text{III}}_5$  resonance excitation of spRR spectrum. However, this peak is not detected and the maximum peak shifts to  $3121 \text{ cm}^{-1}$  in stRR spectra. This demonstrates that the proper choice of the excitation wavelength makes stRR spectroscopy a suitable technique for capturing the rapid structural changes of guanine–cytosine undergone upon protonation or tautomeric transformation events.

In summary, the present UVRR signatures of four guanine–cytosine species exhibit abundant marker Raman bands, which carry rich structure information about the microscopic structure, with specific characteristics that would be helpful for conformer selective detection of short-lived tautomer species in DNA mutations. Both frequency-domain spRR and time-domain stRR features were simulated by *ab initio* studies. These data clearly show the unique UVRR fingerprints of the four species. Although both stRR and spRR induce similar spectral signals, the spectroscopic features excited with different wavelengths of incident lights demonstrate the excitation wavelength selectivity of the RR technique. Moreover, the stRR technique also provides femtosecond scale high temporal resolution, providing the ability to detect specific species during the fast kinetics or dynamics undergone upon protonation or tautomeric transformation events. Combining the fingerprint nature of vibration modes, the chemical-specie dependent selectivity of excitation wavelengths, and the resonance enhancement, our results suggest that spRR and stRR are powerful tools for the chemical identification of various guanine–cytosine pairing patterns at low concentrations or possess short lifetimes. Considering the complexity of the physiological environment, the vibrational modes of these G:C tautomers would be affected by the solution environment. An additional assessment on the effects of hydrogen-bonding with solvent water was performed (Tables S1–S4 in Supporting information). The frequency variations of the vibration features discussed here are not significant and would not alter the qualitative conclusions. By carefully choosing excitation energies, it not only filters out the vibrational modes from the solvents, but also monitors the transient short-lived base pair tautomers in different environments. Combined with other conventional methods of experimental characterization, this technique promises to be a powerful tool to provide direct evidence of critical dynamical details of complex systems involving protonation or tautomerization.

#### Declaration of competing interest

The authors declare that they have no known competing financial interests or personal relationships that could have appeared to influence the work reported in this paper.

#### Acknowledgments

We acknowledge the financial support from the National Key Research and Development Program of China (No. 2019YFA0708703), the National Natural Science Foundation of China (NSFC, No. 21773309), the High-level Science Foundation

of Qingdao Agricultural University (No. 663/1114351), the Hefei National Laboratory for Physical Sciences at the Microscale (No. KF2020004), Xiangyang Science and Technology Research and Development (No. 2020YL09) and Hubei University of Arts and Science (Nos. HLOM222003, 2020kypyt002).

### Supplementary materials

Supplementary material associated with this article can be found, in the online version, at doi:10.1016/j.ccl.2023.108144.

### References

- [1] J.D. Watson, F.H.C. Crick, *Nature* 171 (1953) 737–738.
- [2] M. D.Tapal, J.R. Fresco, *Nature* (1976) 285–289.
- [3] B. Sathyamoorthy, H. Shi, H. Zhou, et al., *Nucleic Acids Res.* 45 (2017) 5586–5601.
- [4] L. Slocombe, M. Sacchi, J. Al-Khalili, *Commun. Phys.* 5 (2022) 109.
- [5] J.D. Watson, F.H.C. Crick, *Nature* 171 (1953) 964–967.
- [6] K. Umetsaki, K. Odai, *J. Phys. Chem.* 124 (2020) 1715–1722.
- [7] L.Y. Fu, G.Z. Wang, B.G. Ma, H.Y. Zhang, *Biochem. Biophys. Res. Commun.* 409 (2011) 367–371.
- [8] O.O. Brovarets, A. Muradova, D.M. Hovorun, *Front. Chem.* 8 (2020) 574454.
- [9] H.S. Alvey, F.L. Gottardo, E.N. Nikolova, H.M. Al-Hashimi, *Nat. Commun.* 5 (2014) 4786.
- [10] R. Srivastava, *Front. Chem.* 7 (2019) 536.
- [11] O. Pusuluk, G. Torun, C. Deliduman, *Mod. Phys. Lett. B* 32 (2018) 1850308.
- [12] L. Slocombe, M. Winokan, J. Al-Khalili, M. Sacchi, *Commun. Chem.* 5 (2022) 144.
- [13] A.L. Stelling, A. Liu, W. Zeng, et al., *Angew. Chem. Int. Ed.* 58 (2019) 12010–12013.
- [14] C.M. Muntean, N.E. Dina, I. Bratu, et al., *Spectrochim. Acta A: Mol. Biomol. Spectrosc.* 258 (2021) 119866.
- [15] J. Liu, Y. Chen, F. Li, et al., *Fundam. Res* 1 (2021) 747–751.
- [16] J.J. Park, C.S. Lee, S.Y. Han, *J. Am. Soc. Mass Spectrom.* 29 (2018) 2368–2379.
- [17] E.N. Nikolova, F.L. Gottardo, H.M. Al-Hashimi, *J. Am. Chem. Soc.* 134 (2012) 3667–3670.
- [18] I.J. Kimsey, E.S. Szymanski, W.J. Zahurancik, et al., *Nature* 554 (2018) 195–201.
- [19] V. Kumar, T. Holtum, J. Voskuhl, et al., *Spectrochim. Acta Part A: Mol. Biomol. Spectrosc.* 254 (2021) 119622.
- [20] L. Chen, Y. Wang, X. Zhao, et al., *J. Mater. Sci. Technol.* 110 (2022) 128–135.
- [21] H. Peng, J. Ren, Y. Wang, et al., *Nano Energy* 88 (2021) 106307.
- [22] Q. Wang, Q. Feng, Y. Lei, et al., *Nat. Commun.* 13 (2022) 3689.
- [23] L. Yang, C. Wang, W. Dai, *Fundam. Res.* 2 (2022) 184–192.
- [24] L. Wang, S. Jiang, Q. Zhang, Y. Luo, *Chin. J. Chem. Phys.* 33 (2020) 680–685.
- [25] H. Ren, Q. Zhang, Z. Wang, et al., *Proc. Natl. Acad. Sci. U. S. A.* 119 (2022) e2202713119.
- [26] H. Ren, H. Li, Q. Zhang, et al., *Fundam. Res.* 1 (2021) 488–494.
- [27] B. Tian, S. Li, S. Lei, et al., *Chin. Chem. Lett.* 32 (2021) 2469–2473.
- [28] Z. Wang, J. Jiang, Y. Huang, et al., *Chin. J. Chem. Phys.* (2022), doi:10.1063/1674-0068/cjcp2203046.
- [29] H. Ren, J.D. Biggs, S. Mukamel, *J. Raman Spectrosc.* 44 (2013) 544–559.
- [30] H. Ren, Z. Wang, S. Guo, et al., *J. Chem. Phys.* 155 (2021) 174301.
- [31] H. Ren, J. Jiang, S. Mukamel, *J. Phys. Chem. B* 115 (2011) 13955–13962.
- [32] B. Tian, C. Cheng, T. Yue, et al., *Chem. Phys.* 513 (2018) 1–6.
- [33] H. Ren, Y. Zhang, S. Guo, et al., *Phys. Chem. Chem. Phys.* 19 (2017) 31103–31112.
- [34] J.P. Merrick, D. Moran, L. Radom, *J. Phys. Chem. A* 111 (2007) 11683–11700.
- [35] R. Bauernschmitt, R. Ahlrichs, *Chem. Phys. Lett.* 256 (1996) 454–464.
- [36] H. Asami, H. Saigusa, J. Kohno, *Chem. Phys. Lett.* 756 (2020) 137828.
- [37] R.L. Martin, *J. Chem. Phys.* 118 (2003) 4775–4777.
- [38] F. Qiu, Z.Y. Gong, D. Cao, et al., *JACS Au* 2 (2022) 150–158.
- [39] H.F. Ma, Y.Z. Yang, H. Jing, et al., *Chin. J. Chem. Phys.* 36 (2023) 15–24.
- [40] V. Barone, M. Cossi, *J. Phys. Chem. A* 102 (1998) 1995–2001.
- [41] A.F. Cruz-Ortiz, M. Rossa, F. Berthias, et al., *J. Phys. Chem. Lett.* 8 (2017) 5501–5506.
- [42] J.J. Park, S.Y. Han, *J. Am. Soc. Mass Spectrom.* 30 (2019) 846–854.
- [43] Z. Wen, G.J. Thomas, *Biopolymers* 45 (1998) 247–256.
- [44] X. Liu, X. Wei, H. Zhou, et al., *J. Phys. Chem. A* 122 (2018) 5710–5720.
- [45] S. Sasidharanpillai, G.R. Loppnow, *J. Phys. Chem.* 123 (2019) 3898–3906.
- [46] F. D'Amico, P. Zucchiatti, K. Latella, et al., *J. Biophotonics* 13 (2020) e202000150.